Rhbdf2 mutations increase its protein stability and drive EGFR hyperactivation through enhanced secretion of amphiregulin

Vishnu Hosur, Kenneth R. Johnson, Lisa M. Burzenski, Timothy M. Stearns, Richard S. Maser, and Leonard D. Shultz[1]

The Jackson Laboratory, Bar Harbor, ME 04609

Edited by Dennis A. Carson, University of California at San Diego, La Jolla, CA, and approved April 17, 2014 (received for review December 23, 2013)

The rhomboid 5 homolog 2 (*Rhbdf2*) gene encodes an inactive rhomboid (iRhom) protease, iRhom2, one of a family of enzymes containing a long cytosolic N terminus and a dormant peptidase domain of unknown function. iRhom2 has been implicated in epithelial regeneration and cancer growth through constitutive activation of epidermal growth factor receptor (EGFR) signaling. However, little is known about the physiological substrates for iRhom2 or the molecular mechanisms underlying these functions. We show that iRhom2 is a short-lived protein whose stability can be increased by select mutations in the N-terminal domain. In turn, these stable variants function to augment the secretion of EGF family ligands, including amphiregulin, independent of metalloprotease a disintegrin and metalloproteinase 17 (ADAM17) activity. In vivo, N-terminal iRhom2 mutations induce accelerated wound healing as well as accelerated tumorigenesis, but they do not drive spontaneous tumor development. This work underscores the physiological prominence of iRhom2 in controlling EGFR signaling events involved in wound healing and neoplastic growth, and yields insight into the function of key iRhom2 domains.

curly bare | ERAD | tylosis | epithelial cancer | pseudoenzyme

Inactive rhomboids (iRhoms) are highly conserved but proteolytically inactive intramembrane proteins (1). iRhoms are characterized by a long cytosolic N-terminal domain, a conserved cysteine-rich iRhom homology domain (IRHD), and a dormant proteolytic site lacking an active-site serine residue within the peptidase domain (1). Recently, Greenblatt et al. (2) reported that Derlin-1 belongs to the rhomboid family and suggested that a dual role exists for the cytosolic and peptidase domains of this novel rhomboid pseudoprotease. They showed that although the cytosolic domain of Derlin-1 is essential in mammalian cells for clearance of misfolded proteins from the endoplasmic reticulum, the transmembrane domain is required to interact with its substrates (2), suggesting that these two domains have distinctive functions. The physiological significance of these domains is unclear.

Despite their lack of proteolytic activity, iRhoms participate in a diverse range of functions in a variety of species, including regulation of epidermal growth factor receptor (EGFR) signaling in *Drosophila melanogaster* (3), survival of human squamous epithelial cancer cells (4, 5), misfolded protein clearance from endoplasmic reticulum membranes in mammalian cell lines (2), induction of migration in primary mouse keratinocytes (6), secretion of soluble TNF-α in mice (7, 8), and regulation of substrate selectivity of stimulated a disintegrin and metalloproteinase 17 (ADAM17)-mediated metalloprotease shedding in mouse embryonic fibroblasts (MEFs) (6, 9). Although the physiological targets of iRhoms are largely unknown, mounting literature suggests that EGF-like ligands are potential substrates. For example, studies in *D. melanogaster* and in mammalian cell lines showed that iRhoms could negatively regulate EGFR signaling by breaking down EGF-like substrates through endoplasmic reticulum-associated degradation (ERAD) (3).

Recent data also point to a role for iRhoms in EGFR-mediated human neoplastic growth. siRNA-mediated silencing of iRhom1 inhibits tumor growth by inducing apoptosis (4). Likewise, missense mutations in *RHBDF2* (p.I186T, p.P189L, and p.D188N), the gene encoding iRhom2, cause tylosis with human esophageal cancer, which is characterized by palmoplantar and oral hyperkeratosis (10). Other studies have revealed that iRhom1 promotes the survival of epithelial tumors through EGFR transactivation (5), whereas somatic mutations in iRhom2 are strongly linked to gain of EGFR signaling (11). Although the mechanisms underlying the pathogenesis of cancer are evolving, these studies further strengthen the link between iRhoms and EGFR signaling.

Rhomboids have been extensively characterized in *Drosophila*, in which changes in EGFR signaling can be detected by studying the wing phenotype (12, 13), whereas in mice, such alterations can be analyzed by examining hair follicle development (14), response to wound healing (15), and tumorigenesis (16). Here, we show that a spontaneous deletion within the rhomboid 5 homolog 2 (*Rhbdf2*) gene in mice underlies the curly-bare (*cub*) mutation, in which loss of the cytosolic N-terminal domain of iRhom2 causes subsequent effects on hair follicle development, wound healing, and tumorigenesis. We find that iRhom2 is a short-lived protein but that gain-of-function mutations in the N terminus (tylosis) or loss of the N terminus (*cub* mutation) increase mutant protein stability, leading to metalloprotease-independent secretion of the EGFR ligand amphiregulin (AREG). Using a genetic modifier of the *cub* phenotype (*Mcub*), we demonstrate that AREG is a physiological target of iRhom2. We also identify key amino acids in the peptidase domain of iRhom2 that are necessary for AREG secretion, suggesting that the peptidase domain of this pseudoenzyme might be functional de-

Significance

Epidermal growth factor receptor (EGFR) signal transduction plays a major role in growth, proliferation, and differentiation of mammalian cells. Although inactive rhomboids (iRhoms) are cardinal regulators of EGFR signaling in *Drosophila melanogaster*, their physiological role in regulating EGFR signaling and their substrates in mammals remain unclear. Here, we show that iRhoms are short-lived proteins, but dominant mutations increase their protein stability and stimulate secretion of specific EGF family ligand amphiregulin independent of metalloprotease activity. This study demonstrates the significance of mammalian iRhoms in regulating an EGFR signaling event that promotes accelerated wound healing and triggers tumorigenesis. Given their ability to regulate EGFR signaling in parallel with metalloproteases, iRhoms can be potential therapeutic targets in impaired wound healing and cancer.

Author contributions: V.H., R.S.M., and L.D.S. designed research; V.H., K.R.J., and L.M.B. performed research; V.H. contributed new reagents/analytic tools; V.H., K.R.J., T.M.S., R.S.M., and L.D.S. analyzed data; and V.H. and L.D.S. wrote the paper.

The authors declare no conflict of interest.

This article is a PNAS Direct Submission.

[1]To whom correspondence should be addressed. E-mail: lenny.shultz@jax.org.

This article contains supporting information online at www.pnas.org/lookup/suppl/doi:10.1073/pnas.1323908111/-/DCSupplemental.

spite lacking a serine residue in the putative active site. This study therefore yields insight into the function of key iRhom domains and establishes a framework for understanding the relationship between iRhoms, EGFR signaling, and the biological processes involved in wound healing and tumorigenesis.

Results

***cub* Mutation Leads to Hyperactivation of the EGFR Signaling Pathway.** We previously described a recessive mouse mutation named *cub*, which is characterized by a hairless phenotype (17). We previously mapped the *cub* mutation to a locus on distal chromosome (Chr) 11 and mapped a dominant *Mcub* to a 10-cM interval on Chr 5 (17). A single copy of the dominant *Mcub* allele in combination with the *cub*/*cub* genotype results in a full, wavy coat rather than the hairless coat of *cub*/*cub mcub*/*mcub* mice (17). Because of the potential relationship between the hair coat phenotypes and EGFR signaling (18, 19), we investigated whether the *cub*/*cub mcub*/*mcub* genotype might also be associated with other aspects of altered EGFR signaling, such as cell proliferation and cell migration.

We performed proliferation, cell migration (scratch-wound healing), and immunoblot assays on mouse MEFs isolated from *cub*/*cub mcub*/*mcub* and control ($^{+/+}$ *mcub*/*mcub*) mice. The *cub*/*cub mcub*/*mcub* MEFs had significantly higher rates of proliferation and migration relative to control MEFs (Fig. 1 *A* and *B*). These changes were associated with significant increases in the phosphorylation of canonical signal transduction proteins of the EGFR pathway, including, Akt, S6, mTOR, and p38 (Fig. 1*C*). Further, we observed a significant reduction in cell-surface EGFR levels in *cub*/*cub mcub*/*mcub* MEFs (Fig. 1*C*), indicating internalization and constitutive activation of EGFR signaling (20–22).

Because activated EGFR signaling mediates epithelial regeneration (23–25), we examined whether this increase in EGFR signaling corresponds to changes in epithelial proliferation. We conducted wound-healing assays in which we punched 2-mm through-and-through holes into the ears of 6- to 40-wk-old *cub* mice and monitored the rate of closure over subsequent days (Fig. 1 *D*–*F*). Within 14 d, *cub*/*cub mcub*/*mcub* mice showed accelerated closure compared with control $^{+/+}$ *mcub*/*mcub* littermates. The $^{+}$/*cub mcub*/*mcub* mice (which have a normal coat) also showed faster healing 14 d postinjury relative to control mice (Fig. S1 *A* and *B*), suggesting that a single mutant *cub* allele can trigger increased EGFR signaling, although not at levels high enough to block hair follicle induction (17, 26). These data strongly indicate that the *cub*/*cub mcub*/*mcub* genotype results in a hyperactive EGFR phenotype.

***cub* Is a Mutation of the *Rhbdf2* Gene, Encoding iRhom2.** Next, we examined the iRhom2 gene *Rhbdf2* as a candidate for the *cub* mutation because of its coincident position with the *cub* mutation on Chr 11 and the established relationship between rhomboid proteases and EGFR-mediated signaling (3, 6). DNA sequencing of *cub*/*cub* mice identified a 12,681-bp deletion in the *Rhbdf2* gene, which results in loss of exons 2–6 (Fig. 2*A*). To test whether the deletion produces an aberrant *Rhbdf2* transcript, we performed reverse transcriptase (RT) PCR on RNA derived from WT and *cub*/*cub mcub*/*mcub* MEFs using primers designed to amplify exons 2, 5, 12, and 19. As expected from the extent of the genomic deletion, the *cub* transcript contained exons 12 and 19 but lacked exons 2 and 5 (Fig. 2*B*). Further, quantitative RT-PCR (qPCR) on RNA from *cub*/*cub mcub*/*mcub* and $^{+/+}$ *mcub*/*mcub* skin amplified *cub* transcripts in which exons 2–6 were deleted but the remaining exons were expressed, suggesting that the rest of the *cub* gene is transcribed in *cub* mice (Fig. 2*C*). The structure of the *cub* genomic deletion suggests that *cub* transcripts would result in splicing of exons 1–7. To test this interpretation, we performed qPCR with a probe specifically designed to amplify only transcripts containing exon 1 spliced to exon 7. Using this probe, we detected a PCR product in *cub*/*cub*

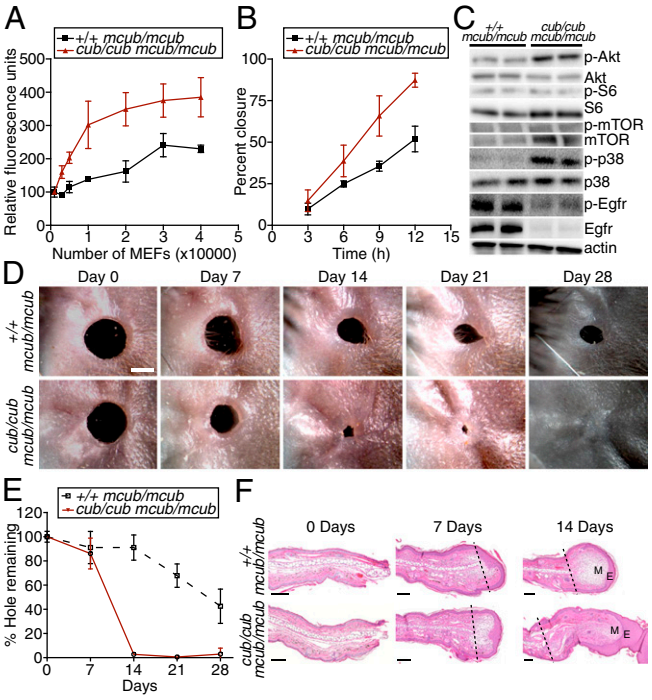

Fig. 1. *cub* mutation accelerates EGFR-related cell proliferation and migration, as well as cutaneous healing. (*A*) Quantitation of MEFs using a proliferation assay (*SI Materials and Methods*). Cells were seeded at the numbers indicated on the *x* axis and incubated for 24 h. The extent of fluorescence is proportional to the amount of total cellular DNA. (*B*) Quantitation of migration of *cub*/*cub mcub*/*mcub* and $^{+/+}$ *mcub*/*mcub* MEFs using a scratch-wound assay (*Materials and Methods*). The width of the scratch wound was measured at time 0 (100% open), and the increase in wound closure at each time point was calculated as a percentage of the original width. (*C*) Immunoblot analysis of *cub*/*cub mcub*/*mcub* or $^{+/+}$ *mcub*/*mcub* MEFs for various markers of EGFR signaling. Cell lysates were run in duplicate. Actin served as a loading control. (*D*) Representative images of regenerating ear tissue in 6- to 40-wk-old female *cub*/*cub mcub*/*mcub* and $^{+/+}$ *mcub*/*mcub* mice (n = 3 per group) at 0, 7, 14, 21, and 28 d postwounding. (Magnification: 4×.) (Scale bar: 1mm.) (*E*) Quantification of ear hole closures shown in *D*. (*F*) Cross-section of ears from *cub*/*cub mcub*/*mcub* and $^{+/+}$ *mcub*/*mcub* mice at 0, 7, and 14 d postwounding stained with H&E. (Magnification: 10×.) (Scale bars: 100 μm.) Notice the undifferentiated and thickened epidermis (E; 10–12 nucleated layers) and the extensive degree of proliferation (M) in the ears of *cub*/*cub mcub*/*mcub* mice. The dotted line indicates the site of excision. Data in *A*, *B*, and *E* are shown as mean ± SD.

mcub/*mcub* mice but not in $^{+/+}$ *mcub*/*mcub* mice (Fig. 2*D*). These findings confirm that *cub* is a mutation of the *Rhbdf2* gene, and it will henceforth be referred to as *Rhbdf2*^{cub}.

Given that the normal translation initiation site in exon 3 is missing in *Rhbdf2*^{cub} transcripts, we next tested whether these mutant transcripts could produce a mutant iRhom2 protein. Sequence analysis of *Rhbdf2*^{cub} DNA revealed that the next in-frame translation initiation site (ATG) was in exon 8, which would result in an ∼63.5-kDa protein. Because we lacked an antibody to iRhom2, we tested whether *Rhbdf2*^{cub} transcripts could produce a protein product in vitro by cloning both full-length WT human *RHBDF2* cDNA (Hu*Wt*) and a version that mimicked the mutant *Rhbdf2*^{cub} transcript (Hu*Cub*) into a C-terminal Flag-tagged expression vector. First, using immunoblotting, we determined that the Hu*Wt* clone generated an ∼100-kDa protein product, whereas the Hu*Cub* mutant construct generated an ∼67-kDa product, consistent with the expected molecular mass of the tagged proteins (Fig. 2*E*). Furthermore, there was no evidence of any shortened protein products in the Hu*Wt* clone. Second, using immunostaining, we examined the

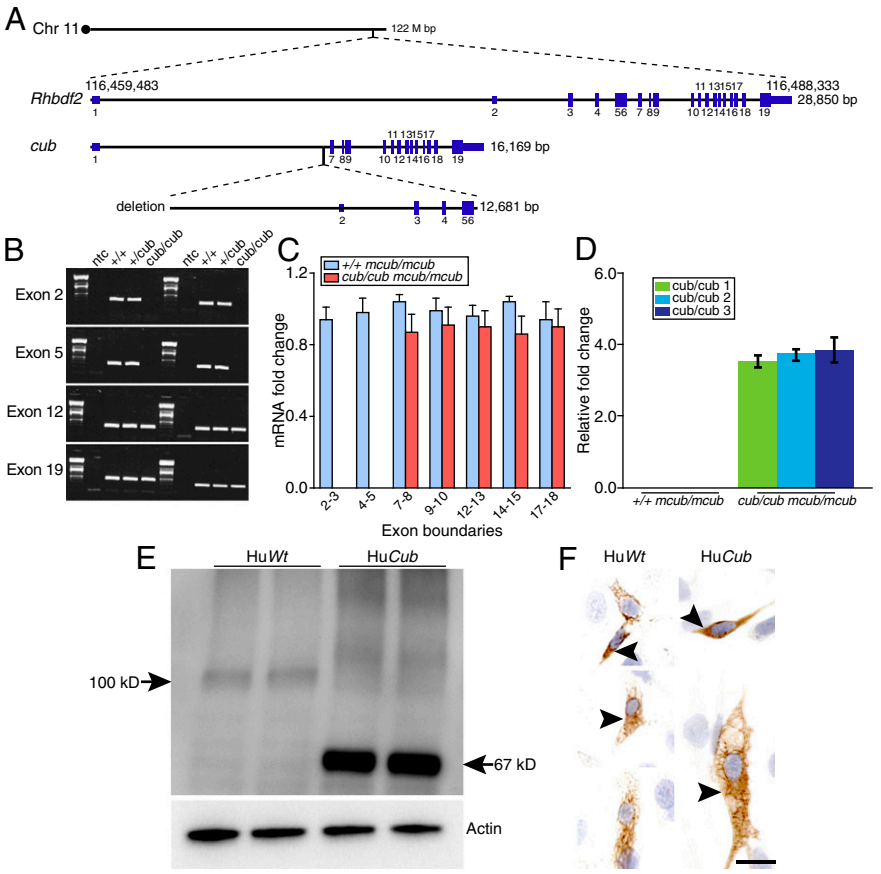

Fig. 2. *cub* is a mutation of the *Rhbdf2* gene. (*A*) *cub* mutation is a 12,681-bp deletion in the mouse *Rhbdf2* gene. The deletion starts midway between exons 1 and 2, and encompasses exons 2–6, ending shortly after exon 6. (*B*) RT-PCR on MEFs from $^{+/+}$ *mcub/mcub*, $^{+}$*/cub mcub/mcub*, and *cub/cub mcub/mcub* mice using primers against exons 2, 5, 12, and 19. ntc, no template control. (*C*) qPCR on cDNA extracted from skin tissues using TaqMan gene expression assays against the indicated exon boundaries. Actin served as an endogenous control. Data are normalized to $^{+/+}$ *mcub/mcub* actin levels. Samples were run in triplicate with four biological replicates. (*D*) qPCR with a custom TaqMan gene expression assay to detect transcripts with an exon 1/exon 7 boundary. Samples were run in triplicate with three biological replicates (each color bar represents an individual mouse) Data in *C* and *D* are shown as mean ± SD. (*E*) Anti-Flag immunoblot of HEK 293 cells transiently expressing Flag-tagged Hu*Wt* (human full-length *RHBDF2* cDNA) and Hu*Cub* (human version of *cub* cDNA). Actin served as a loading control. (*F*) Representative images of Flag-tagged Hu*Wt*- and Hu*Cub*-expressing B6 primary MEFs stained using a Flag-specific antibody (brown). DAPI was used to counterstain the nucleus (blue). Arrowheads represent cytoplasmic expression of both full-length and mutant proteins. (Magnification: 40×.) (Scale bars: 25 μm.)

localization patterns of both forms of protein after transfection of B6 MEFs (Fig. 2*F* and Fig. S2 *A* and *B*) with either the Hu*Wt* or Hu*Cub* clone. Both forms were expressed in the endoplasmic reticulum, and no staining was observed in either the Golgi or nucleus (Fig. S2 *A* and *B*), suggesting that the mutation does not lead to altered protein localization.

Genetic Noncomplementation Confirms That *cub* Is a Mutant Allele of the *Rhbdf2* Gene and a Gain-of-Function Mutation. To examine whether $Rhbdf2^{cub}$ is a gain-of-function mutation rather than a null mutation, we generated *Rhbdf2* KO ($Rhbdf2^{-/-}$) mice using ES cells from the Knockout Mouse Project (KOMP) repository, in which *lacZ* expression is under control of the endogenous *Rhbdf2* promoter (Fig. 3*A*). *Rhbdf2* promoter-driven *lacZ* expression was predominantly observed in the epidermis and the inner and outer sheath layers of hair follicles in the skin (Fig. 3*B*). However, the wound healing (Fig. 3*C*) and loss-of-hair (Fig. 3*D*) phenotypes observed in the $Rhbdf2^{cub/cub}$ mice were not seen in $Rhbdf2^{-/-}$ mice, which appeared otherwise normal. An allele test mating between $Rhbdf2^{cub/cub}$ and $Rhbdf2^{-/-}$ mice yielded compound mutant ($Rhbdf2^{-/cub}$) mice with a sparse hair coat (Fig. 3*E*), indicating genetic noncomplementation and confirming that *cub* is a mutant allele of the *Rhbdf2* gene. Additionally, the level of hair growth in the $Rhbdf2^{-/cub}$ compound mutant mice was intermediate between that of $Rhbdf2^{cub/cub}$ and $Rhbdf2^{+/+}$ or $Rhbdf2^{-/-}$ mice, confirming that expression of the mutant $Rhbdf2^{cub}$ protein product, rather than *Rhbdf2* deficiency, causes the $Rhbdf2^{cub/cub}$ phenotype.

Genetic *Mcub* Is a Loss-of-Function Mutation of the *Areg* Gene. We next sought to map the mutation underlying the $Rhbdf2^{cub}$ modifier gene (*Mcub*). The map position (17) coincides with that of a cluster of four EGFR ligand-encoding genes on Chr 5: *Epng*, *Ereg*, *Areg*, and *Btc*. We considered each of these four genes as candidate loci for the *Mcub* mutation. By sequencing the exons and flanking regions of each gene in *Mcub*/*Mcub* $Rhbdf2^{cub/cub}$ mice (Table S1), we found that *Mcub* is a loss-of-function mutation in *Areg* (Fig. 4*A*), a gene that encodes the autocrine keratinocyte growth factor AREG (27).

Mcub is a T-to-G point mutation that destroys the canonical donor splice site of exon 1 and leads to the exclusive use of an alternative downstream splice site that adds 22 extra nucleotides to the *Areg* transcript; this addition of extra nucleotides disrupts the coding frame and introduces a premature stop codon (Fig. S3). This mutation will henceforth be referred to as $Areg^{Mcub}$. Notably, the hyperactive EGFR signaling (Fig. S4*A*) and the rapid wound closure capability of $Rhbdf2^{cub/cub}$ mice are significantly reduced (Fig. 4 *B* and *C*), and the loss-of-hair phenotype is prevented when a single copy of the dominant $Areg^{Mcub}$ allele is present (17). The dominant $Areg^{Mcub}$ mutation does not confer a normal hair coat to the $Rhbdf2^{cub/cub}$ mice but, rather, a wavy hair phenotype (17), suggesting remaining abnormalities in the EGFR pathway (28).

We next measured serum levels of AREG in $Rhbdf2^{cub/cub}$ $Areg^{+/+}$, $Rhbdf2^{cub/cub}$ $Areg^{Mcub/Mcub}$, and $Rhbdf2^{+/+}$ $Areg^{+/+}$ mice. We found no detectable AREG in the serum of $Rhbdf2^{cub/cub}$ $Areg^{Mcub/Mcub}$ mice, but we did observe a dramatic increase in serum AREG levels in $Rhbdf2^{cub/cub}$ $Areg^{+/+}$ mice compared with $Rhbdf2^{+/+}$ $Areg^{+/+}$ mice (Fig. 4*D*). Measurements of supernatant AREG levels from cultured mouse epidermal keratinocytes of $Rhbdf2^{cub/cub}$ $Areg^{+/+}$, $Rhbdf2^{cub/cub}$ $Areg^{Mcub/Mcub}$, and $Rhbdf2^{+/+}$ $Areg^{+/+}$ mice yielded similar results (Fig. 4*E*). AREG is abundantly expressed in normal skin (29); therefore, we next performed qPCR on skin samples from $Rhbdf2^{cub/cub}$ $Areg^{+/+}$ and $Rhbdf2^{+/+}$ $Areg^{+/+}$ mice to measure transcript levels of *Areg*, as well as six other genes known to encode EGFR ligands (*Egf*, *Tgfα*,

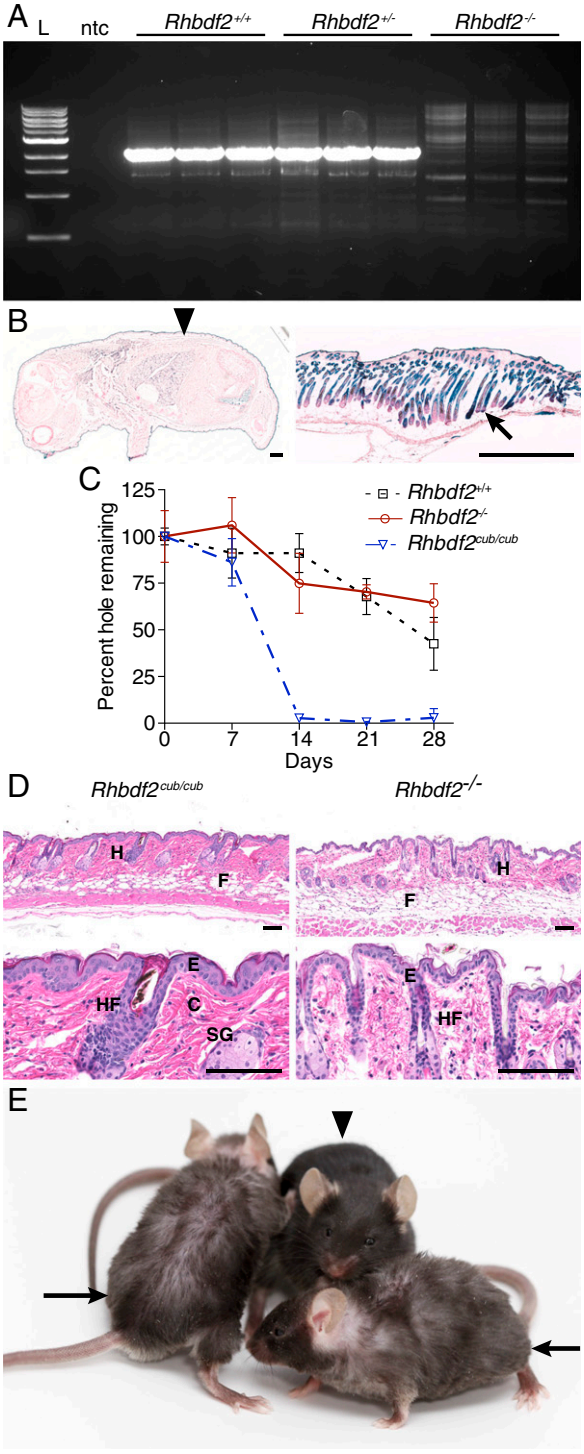

Fig. 3. *Rhbdf2*^{cub} is a gain-of-function mutation rather than a null mutation. (*A*) PCR for WT product in KOMP *Rhbdf2* KO mice. The expected product is 2,181 bp. L, New England Biolabs 1-kb DNA ladder. (*B*) Reporter gene analysis of *Rhbdf2* expression. A whole-mount X-gal–stained embryonic day 18.5 *Rhbdf2*$^{-/-}$ embryo shows strong expression of β-gal in the epidermis (arrowhead), and X-gal–stained 2-wk-old female *Rhbdf2*$^{-/-}$ skin shows β-gal positivity in the inner and outer sheath layers of hair follicles (arrow). (Magnification: 2.5× and 5×, respectively.) No staining was observed in the hair shaft. (Scale bars, 1 mm.) (*C*) Mice with a null mutation of *Rhbdf2* lack a regenerative phenotype as demonstrated by significantly delayed wound closure in the ears of 6- to 8-wk-old female *Rhbdf2*$^{-/-}$ mice compared with those of *Rhbdf2*$^{cub/cub}$ mice. (*D*) Mice with a null mutation of *Rhbdf2* have normal skin and hair morphology. H&E-stained sections of adult skin from *Rhbdf2*$^{cub/cub}$ and *Rhbdf2*$^{-/-}$ mice were taken at the indicated times after wounding. The adult *Rhbdf2*$^{cub/cub}$ skin displays a thin hypodermal fat layer (F), abnormal hair follicles (H), thick epidermis (E), enlarged sebaceous glands (SG), dense interlacing bundles of collagen fibers (C), and no full differentiation of hair follicles and hair bulb (HF). The adult *Rhbdf2*$^{-/-}$ skin shows normal epidermis and hair follicles. (Scale bars, 100 μm.) (Magnification: 10× and 40×, respectively.) (*E*) *Rhbdf2*$^{-/-}$ mice develop a normal hair coat (arrowhead), whereas compound mutant *Rhbdf2*$^{-/cub}$ mice exhibit a sparse hair coat (arrow).

Btc, *Epgn*, *Ereg*, and *Hbegf*). Compared with controls, we observed a fourfold increase in *Areg*, and subtle but statistically significant increases in *Epgn* and *Hbegf* mRNAs, in *Rhbdf2*$^{cub/cub}$ *Areg*$^{+/+}$ mice. Also, there was a statistically significant decrease in *Btc* and *Egf* transcript levels (Fig. 4*F*).

Lastly, to examine whether AREG mediates the hyperactive EGFR phenotype, we silenced *Areg* expression in *Rhbdf2*$^{+/+}$ and *Rhbdf2*$^{cub/cub}$ MEFs (Fig. S4*B*) using lentiviral shRNA and performed proliferation assays. Whereas silencing of *Areg* had a subtle effect on proliferation of *Rhbdf2*$^{+/+}$ MEFs (Fig. S4*C*), proliferation rates of *Rhbdf2*$^{cub/cub}$ MEFs were significantly reduced (Fig. S4*D*). Taken together, these data suggest that enhanced AREG levels mediate the mutant phenotype of the *Rhbdf2*$^{cub/cub}$ mice via a gain of EGFR signaling. Our findings are consistent with previous reports showing that exposure to high concentrations of AREG influences hair follicle development (26, 27) and tissue regeneration (30, 31). Furthermore, our data reveal that the *Rhbdf2*^{cub} phenotype is modified by *Areg*^{Mcub} expression.

N-terminal–Truncated iRhom2 Induces Substrate-Specific Secretion of EGFR Ligands Independent of ADAM17. Nakagawa et al. (32) found that N-terminal–truncated but not full-length iRhom1 induces heparin-binding (HB) EGF secretion in *Drosophila*. Moreover, recent evidence suggests that active rhomboid proteases, with short or nonexistent N-terminal domains, cleave membrane-tethered EGF independent of metalloprotease activity (33). Thus, we asked whether *Rhbdf2*^{cub}, with its short N-terminal domain, could induce secretion of AREG independent of metalloprotease activity. We performed in vitro cleavage assays in the presence or absence of marimastat (MM), a potent broad-spectrum metalloprotease inhibitor that can block both ADAM17- and ADAM10-dependent shedding of substrates (34, 35). Because of the significant homology between the mouse and human *RHBDF2* genes (3, 32, 33, 36), we transfected 293T cells with human *AREG* either alone or with the Hu*Wt* or Hu*Cub* *RHBDF2* gene (Fig. 5*A*) and measured AREG levels in conditioned medium. In the absence of MM, we observed no difference in AREG levels between *AREG*-expressing and *AREG*/Hu*Cub*-coexpressing cells, whereas coexpression of Hu*Wt* and *AREG* reduced AREG levels by ∼60% (Fig. 5*B*). Intriguingly, in the presence of MM, AREG levels were approximately twofold higher in Hu*Cub*/*AREG*-cotransfected cells compared with cells transfected with Hu*Wt* and *AREG* or *AREG* alone (Fig. 5*B*). These data suggest that N-terminal–truncated iRhom2 can enhance AREG secretion, which only becomes apparent when metalloprotease activity is diminished.

iRhom2 has been shown to regulate maturation of ADAM17 and, in turn, ADAM17-dependent shedding (7, 8, 37). Because *Rhbdf2*^{cub} is a gain-of-function mutation rather than a null mutation, there is a possibility that *Rhbdf2*^{cub} could enhance ADAM17 activity, and thereby increase AREG secretion. ADAM17 activity can be measured in mice by examining TNF-α secretion after stimulation with bacterial endotoxin LPS (7, 8). We therefore used this approach to test changes in ADAM17 activity in *Rhbdf2*^{cub} mice by injecting LPS into *Rhbdf2*$^{cub/cub}$, *Rhbdf2*$^{-/-}$, and *Rhbdf2*$^{+/+}$ mice and measuring serum TNF-α levels. We

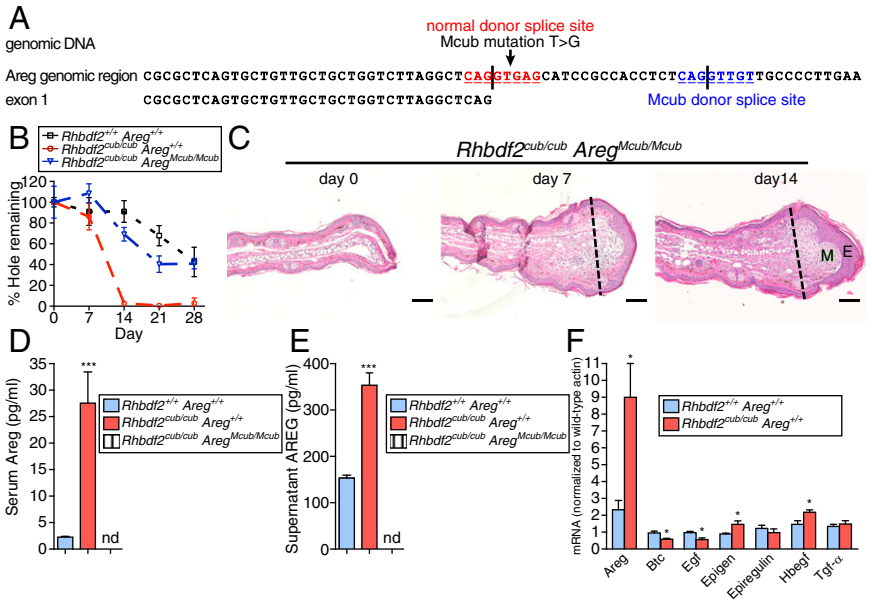

Fig. 4. *Mcub* is a mutation of the *Areg* gene. (*A*) *Mcub* is a T-to-G point mutation that disrupts the normal donor splice site (exon 1) in the *Areg* gene, causing the use of an alternative downstream splice site. (*B*) Healing of ear holes in 6- to 8-wk-old female *Rhbdf2*$^{+/+}$ *Areg*$^{+/+}$, *Rhbdf2*$^{cub/cub}$ *Areg*$^{+/+}$, and *Rhbdf2*$^{cub/cub}$ *Areg*$^{Mcub/Mcub}$ mice (n = 3 mice per group) over a period of 28 d. Data are shown as mean ± SD. (*C*) H&E-stained sections show postexcision healing of ear holes of *Rhbdf2*$^{cub/cub}$ *Areg*$^{Mcub/Mcub}$ mice. The dotted line indicates the site of excision. (Magnification: 10×.) (Scale bars: 100 μm.) E, epidermis; M, proliferation. Compare with Fig. 1*F*. (*D*) Serum AREG levels in age-matched *Rhbdf2*$^{+/+}$ *Areg*$^{+/+}$, *Rhbdf2*$^{cub/cub}$ *Areg*$^{+/+}$, and *Rhbdf2*$^{cub/cub}$ *Areg*$^{Mcub/Mcub}$ female mice. AREG was not detected (nd) in the serum of *Rhbdf2*$^{cub/cub}$ *Areg*$^{Mcub/Mcub}$ mice. ***$P < 0.001$. (*E*) ELISA quantitation of AREG levels in the supernatants of cultured mouse epidermal keratinocytes (MEKs) isolated from *Rhbdf2*$^{+/+}$ *Areg*$^{+/+}$, *Rhbdf2*$^{cub/cub}$ *Areg*$^{+/+}$, and *Rhbdf2*$^{cub/cub}$ *Areg*$^{Mcub/Mcub}$ mice. AREG was not detected in MEKs from *Rhbdf2*$^{cub/cub}$ *Areg*$^{Mcub/Mcub}$ mice. ***$P < 0.001$. (*F*) qPCR of EGFR ligands: cDNA was extracted from skin tissues of *Rhbdf2*$^{cub/cub}$ *Areg*$^{+/+}$ and *Rhbdf2*$^{+/+}$ *Areg*$^{+/+}$ mice using TaqMan gene expression assays. Actin served as an endogenous control. Data are normalized to *Rhbdf2*$^{+/+}$ *Areg*$^{+/+}$ actin levels. *$P < 0.05$. Data in *D*–*F* are shown as mean ± SD of three independent experiments.

found that both LPS-injected *Rhbdf2*$^{cub/cub}$ and *Rhbdf2*$^{-/-}$ mice had a markedly lower induction of TNF-α relative to LPS-injected *Rhbdf2*$^{+/+}$ mice (Fig. 5*C*). These results suggest that ADAM17 activity is significantly attenuated in *Rhbdf2*$^{cub/cub}$ and *Rhbdf2*$^{-/-}$, and they also implicate a role for the N-terminal domain of iRhom2 in regulation of ADAM17-dependent TNF-α release. Notably, serum TNF-α levels in LPS-stimulated *Rhbdf2*$^{cub/cub}$ mice were not completely abrogated, suggesting that ADAM17 activity is attenuated but not eliminated (38). The observation that ADAM17 activity is attenuated in *Rhbdf2*$^{cub/cub}$ mice explains the nonlethal or noninflammatory cutaneous phenotype in *Rhbdf2*$^{-/-}$ and *Rhbdf2*$^{cub/cub}$ mice compared with *Adam17*$^{-/-}$ mice (39, 40) or with transgenic mice overexpressing AREG (41).

We next sought to assess the protease selectivity of the active rhomboid proteases for other EGF-like substrates, and whether these differed from Hu*Cub*. In accordance with a previous study (33), we found that RHBDL2 selectively increased secretion of EGF but not AREG or HB-EGF compared with empty vector-transfected controls (Fig. 5*D*). In contrast, Hu*Cub* selectively increased secretion of AREG and HB-EGF but not EGF compared with empty vector-transfected cells (Fig. 5 *E*–*G*). These results suggest that the rhomboid peptidase domain confers substrate selectivity. The ability of N-terminal–truncated iRhom1 to induce AREG but not EGF secretion is consistent with this assertion (Fig. S5 *A* and *B*).

To determine how the iRhom2 peptidase domain helps to regulate the secretion of EGF-like substrates, we initially aligned sequences for amino acids of the peptidase domains of human and mouse iRhoms. We found a significant difference in protein sequence homology between the peptidase domains of human iRhom2 and RHBDL2 (Fig. S5*C*). By contrast, the peptidase domains of iRhom1 and iRhom2 show 96% homology. Together, these data suggest that the residues that form the active site or play a role in substrate recognition differ significantly between active rhomboids and iRhoms. In addition, we found that deletion of the Hu*Cub* peptidase domain significantly diminished AREG secretion compared with native Hu*Cub* (Fig. 5*G*), suggesting that the peptidase domain is essential for secretion of EGF-like substrates. To identify the critical residues, we performed site-directed mutagenesis such that key residues in the Hu*Cub* peptidase domain were mutated to alanines. We found that glutamine-426 and cysteine-C432 in transmembrane domain 4, and histidine-366 and histidine-475 in transmembrane domains 2 and 6, respectively, were critical not only for mediating enhanced secretion of AREG/HB-EGF but also for suppression of EGF (Fig. 5 *H* and *I*). However, mutations in serines S362A, 402A, and 425A; glutamic acid E436A; and glutamine Q439A did not alter AREG secretion (Fig. S5*D*). Together, these results suggest that key residues (Fig. 5*J* and Fig. S5*E*) in the peptidase domain of N-terminal–truncated iRhom regulate the secretion of EGF-like substrates independent of metalloprotease activity.

N-Terminal–Truncated iRhom2 Increases Susceptibility to Epithelial Cancers. Two recent studies indicated that missense mutations in *RHBDF2* (p.I186T, p.P189L, and p.D188N) underlie a familial tylosis with esophageal cancer syndrome in families in the United States, United Kingdom, Germany, and Finland (11, 42). Based on our results on *Rhbdf2*^{cub} mutant mice, we predicted that increased AREG secretion due to dominant N-terminal mutations in *RHBDF2* might drive these human pathological changes. We first tested this hypothesis in vitro by coexpressing *AREG* with a Hu*Wt* clone containing the human missense mutation (*RHBDF2* p.I186T) (11), Hu*Cub*, or Hu*Wt* in 293T cells. As expected, expression of the *RHBDF2* p.I186T or Hu*Cub* resulted in greater levels of AREG in conditioned

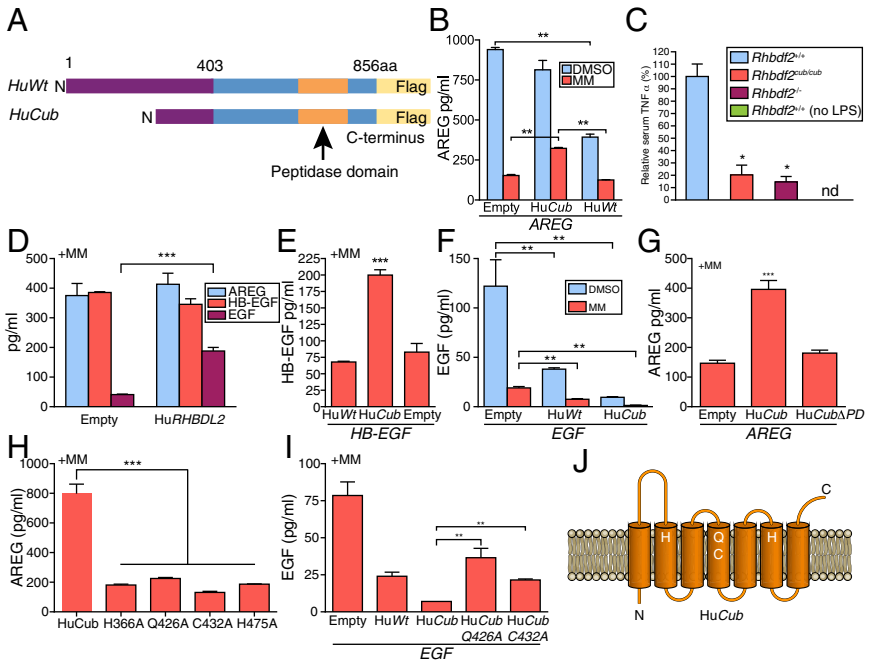

Fig. 5. *Rhbdf2*^{cub} regulates substrate-specific production of EGFR ligands. (*A*) Schematic representation of the Hu*Wt* gene and the Hu*Cub* gene. (*B*) ELISA quantitation of cleaved AREG after coexpression of Hu*Wt* or Hu*Cub* with the *AREG* gene in 293T cells. At 24 h posttransfection, cells were incubated with either DMSO or 10 μM MM for 24 h and AREG levels were analyzed in the conditioned medium. Transfections were performed in duplicate, and the conditioned medium was diluted fivefold. (*C*) Quantitation of serum TNF-α levels by ELISA, 3 h after LPS injection of 8- to 12-wk-old female mice of the indicated genotypes. TNF-α was not detected in the serum of *Rhbdf2*$^{+/+}$ mice with no LPS injection. *$P < 0.05$. (*D*) ELISA quantitation of cleaved AREG/HB-EGF/EGF after coexpression of the human *RHBDL2* (Hu*RHBDL2*) gene with the *AREG*, *HB-EGF*, or *EGF* gene. At 24 h posttransfection, cells were incubated with 10 μM MM for 24 h and AREG/HB-EGF/EGF levels were analyzed in the conditioned medium. Whereas HB-EGF and EGF conditioned media were undiluted, AREG medium was diluted fivefold. Data represent mean ± SD of three independent experiments. ***$P < 0.001$. (*E*) ELISA quantitation of cleaved HB-EGF after coexpression of Hu*Wt* or Hu*Cub* with the *HB-EGF* gene in 293T cells. At 24 h posttransfection, cells were incubated with 10 μM MM for 24 h and HB-EGF levels were analyzed in the conditioned medium. ***$P < 0.001$. (*F*) ELISA quantitation of cleaved EGF after coexpression of Hu*Wt* or Hu*Cub* with the *EGF* gene in 293T cells. At 24 h posttransfection, cells were incubated with either DMSO or 10 μM MM for 24 h and EGF levels were analyzed in the conditioned medium. **$P < 0.01$. (*G*) ELISA quantitation of cleaved AREG after coexpression of Hu*Cub or* Hu*Cub* without the peptidase domain (Hu*CubΔPD*) with the *AREG* gene in 293T cells. At 24 h posttransfection, cells were incubated with 10 μM MM for 24 h and AREG levels were analyzed in the conditioned medium. ***$P < 0.001$. (*H*) ELISA quantitation of cleaved AREG after coexpression of Hu*Cub or* Hu*Cub* with individual alanine mutations with the *AREG* gene in 293T cells. At 24 h posttransfection, cells were incubated with 10 μM MM for 24 h and AREG levels were analyzed in the conditioned medium. ***$P < 0.001$. (*I*) ELISA quantitation of cleaved EGF after coexpression of Hu*Wt*, Hu*Cub*, or Hu*Cub* with individual alanine mutations with the *EGF* gene in 293T cells. At 24 h posttransfection, cells were incubated with 10 μM MM for 24 h and EGF levels were analyzed in the conditioned medium. **$P < 0.001$. (*J*) Membrane topology of *Rhbdf2*$^{cub.}$ The amino acids shown are critical for regulation of EGFR ligand production by *Rhbdf2*^{cub}.

medium and lower intracellular levels compared with Hu*Wt* (Fig. 6 *A* and *B*). Further, *RHBDF2* p.I186T produced AREG levels comparable to those produced by Hu*Cub*, suggesting that loss of, or dominant mutations in, the iRhom2 N terminus lead to increased AREG secretion. Additionally, we found that loss of at least one of four critical residues (H, C, Q, and H) in the peptidase domain of the *RHBDF2* p.I186T mutant resulted in significantly decreased AREG secretion (Fig. 6*C*).

To determine whether the *Rhbdf2*^{cub} allele increases tumor susceptibility, we investigated how its expression would affect adenoma formation in *Apc*$^{Min/+}$ mice, a mouse model of human familial adenomatous polyposis. In *Apc*$^{Min/+}$ mice, spontaneous loss of one WT *Apc* allele induces intestinal epithelial adenoma formation and premature death at a median age of 169 d (43). Notably, *Rhbdf2* (Fig. 6*D*) and *Areg* (31) expression is observed in the small intestine, suggesting a potential functional relationship. We generated and observed *Apc*$^{Min/+}$ *Rhbdf2*$^{+/cub}$ and *Apc*$^{Min/+}$ *Rhbdf2*$^{+/+}$ mice, but because of increased lethality, we could not generate enough *Apc*$^{Min/+}$ *Rhbdf2*$^{cub/cub}$ mice for meaningful comparison. Nonetheless, we did observe a significant difference in the median survival age of *Apc*$^{Min/+}$ *Rhbdf2*$^{+/+}$ (172 d) and *Apc*$^{Min/+}$ *Rhbdf2*$^{+/cub}$ (135 d) mice (Fig. 6*E*). Necropsy of *Apc*$^{Min/+}$ *Rhbdf2*$^{+/+}$ and *Apc*$^{Min/+}$ *Rhbdf2*$^{+/cub}$ mice at 3 mo of age revealed that the presence of a single *Rhbdf2*^{cub} allele significantly increased the number of polyps (Fig. 6 *F* and *G*) and adenoma size (Fig. 6 *F* and *H*) in *Apc*$^{Min/+}$ mice, suggesting that the *cub* mutation increases the growth of epithelial tumors. However, there was no spontaneous incidence of cancer in *Rhbdf2*$^{cub/cub}$ mice aged up to 2 y, suggesting that *Rhbdf2*^{cub} mutation creates a conducive environment for, but alone does not drive, tumor development.

Loss of the Cytosolic N Terminus or Dominant Mutations in the N Terminus of the *RHBDF2* Gene Increase Its Protein Stability. iRhom2 negatively regulates EGFR signaling by promoting degradation of EGF-like ligands through the proteasomal pathway (3). Moreover, we observed that iRhoms induce secretion of AREG/HB-EGF when the cytosolic N terminus is lacking (Fig. 5). Thus, we asked whether gain-of-function mutations in the amino terminus of iRhom2 interfere with proteasomal processing, and thereby increase its stability. We initially examined whether the tylotic *RHBDF2* mutant p.I186T has an ability to interact with AREG. We found that similar to Hu*Wt* and Hu*Cub*, p.I186T forms physical complexes with AREG (Fig. 7*A*). We then compared the protein expression levels of Hu*Wt*, Hu*Cub*, and p.I186T in 293T and COS7 cells by immunocytochemistry and flow cytometry. We observed that Hu*Wt* protein expression was significantly lower compared with both Hu*Cub* and p.I186T ex-

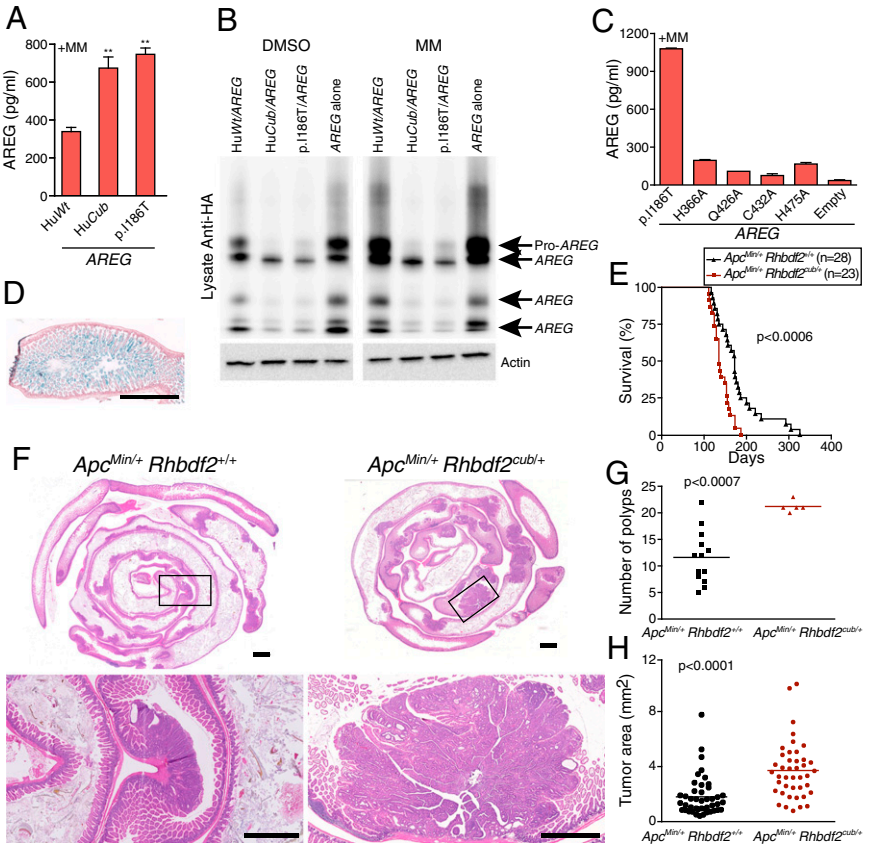

Fig. 6. Heterozygosity of *Rhbdf2*^{cub} results in increased adenoma formation and decreased survival in *Apc*$^{Min/+}$ mice. (*A*) Quantitation of cleaved AREG by ELISA from conditioned medium of HEK 293 cells transfected with *AREG* and the human *RHBDF2* p.I186T mutant, Hu*Wt*, or Hu*Cub* in the presence of 10 μM MM. $^{**}P < 0.01$. (*B*) Western blot of HEK 293 cells cotransfected with *AREG* and Hu*Cub*, Hu*Wt*, or p.I186T; incubated with DMSO or MM; and immunoblotted for HA-AREG. Coexpression of *AREG* and either Hu*Cub* or p.I186T significantly reduces the intracellular levels of pro-AREG compared with those of *AREG*/Hu*Wt* or *AREG* alone, even in the presence of 10 μM MM. (*C*) AREG levels in cells expressing various *RHBDF2 P.I186T* point mutants and cotransfected with the *AREG* gene or empty vector. Each residue was mutated to alanine. Cells were incubated with 10 μM MM for 24 h and assayed for AREG levels in conditioned medium. (*D*) X-gal–stained 2-wk-old female *Rhbdf2*$^{-/-}$ intestine reveals reporter gene β-gal expression in the middle and upper villous regions. (Magnification: 2.5×.) (Scale bar: 1mm.) (*E*) Kaplan–Meier survival curves of *Apc*$^{Min/+}$ *Rhbdf2*$^{+/+}$ ($n = 28$) and *Apc*$^{Min/+}$ *Rhbdf2*$^{+/cub}$ ($n = 23$) mice. The median survival of *Apc*$^{Min/+}$ *Rhbdf2*$^{+/+}$ mice was 172 d, compared with 135 d for *Apc*$^{Min/+}$ *Rhbdf2*$^{+/cub}$ mice. (*F*) H&E-stained sections of intestinal tissue from mice of the indicated genotypes at 3 mo of age. (Magnification: 2.5×.) (Scale bars: 1mm.) Number (*G*) and size (*H*) of polyps per mouse of the indicated genotypes of mice at 3 mo of age are shown. The mean number of polyps in *Apc*$^{Min/+}$ *Rhbdf2*$^{+/+}$ mice was 12, whereas in *Apc*$^{Min/+}$ *Rhbdf2*$^{+/cub}$ mice, the mean number of polyps was 21. The mean tumor sizes were 1.8 mm^2 and 3.7 mm^2 for *Apc*$^{Min/+}$ *Rhbdf2*$^{+/+}$ and *Apc*$^{Min/+}$ *Rhbdf2*$^{+/cub}$ mice, respectively.

pression (Fig. 7 *B* and *C*). Further, when we subjected COS7 cells to a cycloheximide (a protein synthesis inhibitor) chase for the indicated times, within 1 h, we observed an ∼50% reduction in immunoreactivity for Hu*Wt* compared with either Hu*Cub* or the p.I186T (Fig. 7 *D* and *E*). Endoplasmic reticulum-localized rhomboid proteases interact with the ubiquitin proteasome system to promote ERAD (2, 3, 36). Because iRhom2 participates in ERAD, it is possible that it could be a target of proteasomal degradation. We determined the protein $t_{1/2}$ of Hu*Wt* and Hu*Cub* in the presence of a potent proteasomal inhibitor, MG-132. Expectedly, the protein $t_{1/2}$ of Hu*Wt*, but not Hu*Cub*, was significantly increased (Fig. 7*F*), suggesting that the proteasomal degradation of iRhom2 might be affecting its protein stability. We conclude that missense mutations in the amino terminus of iRhom2, similar to the *Rhbdf2*^{cub} mutation, increase its stability and contribute to enhanced AREG secretion independent of metalloprotease activity.

Discussion

The EGFR signal transduction pathway plays an essential role in growth, proliferation, and differentiation of mammalian cells. Canonical EGFR ligands, including EGF, AREG, and HB-EGF, exist as proproteins expressed at the cell surface that, to bind EGFRs, must be shed into the extracellular compartment. Different classes of proteases cleave membrane-tethered EGFR proligands to regulate a broad range of biological activities during various stages of development. Here, we report that iRhom2, a member of a family of rhomboid proteases well known as regulators of EGFR signaling in *Drosophila*, has an ability to regulate EGFR signaling during cutaneous healing and tumor development. We show that iRhom2 is a short-lived protein whose stability can be increased by select mutations in the N-terminal domain. In turn, these stable variants function to enhance AREG secretion independent of metalloprotease activity. We identify an important role for iRhoms in EGFR-dependent cell proliferation and wound healing, and show how iRhom2 mutations that increase EGFR signaling, under the right circumstances, can promote cancer development.

N-Terminal and Peptidase Domains Have Separate Functions in Regulating EGFR Signaling. iRhoms are complex multidomain enzymes that contain a long cytosolic N terminus, a dormant peptidase domain, and a conserved IRHD; the function of these domains remains unknown. Under normal circumstances, iRhoms

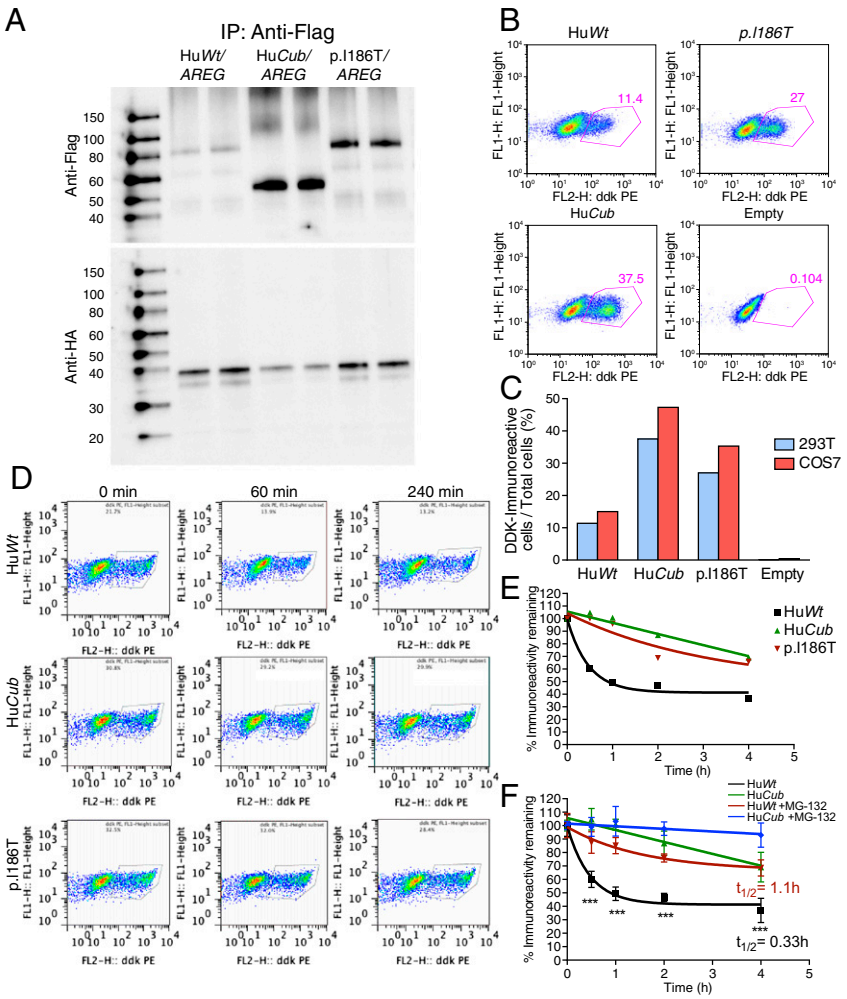

Fig. 7. Mammalian iRHOM2 is a short-lived protease. (*A*) Coimmunoprecipitation (IP) of human iRhom2–AREG complex. Lysates from COS7 cells cotransfected with Flag-tagged Hu*Wt* or Flag-tagged Hu*Cub* or with Flag-tagged p.I186T and HA-tagged *AREG* were immunoprecipitated with anti-Flag magnetic beads and probed with anti-Flag and anti-HA antibodies. (*B*) Flow cytometry results from 293T or COS7 (Fig. S6) cells transfected with the indicated Flag (FL)-tagged genes and immunolabeled using a Flag-specific PE-labeled antibody. Cells were immunolabeled 48 h posttransfection. ddk, also known as Flag. (*C*) Quantification of the data obtained in *B*. (*D*) Transiently transfected COS7 cells were subjected to a chase with 150 μg/mL cycloheximide (the protein synthesis inhibitor) for the indicated times and evaluated for protein expression using Flag-specific PE-labeled antibody. Data are representative of one of a total of three experiments. (*E*) Quantification of the data obtained in *D*. (*F*) Transiently transfected COS7 cells were preincubated for 4 h with 10 μM MG-132, a cell-permeable protease inhibitor, followed by a chase with 150 μg/mL cycloheximide in the presence of MG-132 for the indicated times. Protein expression was determined as described in *D*. ***$P < 0.001$.

negatively regulate EGFR signaling by promoting the degradation of EGF-like substrates (3). However, the *Rhbdf2*^{cub} mutation is unlikely to be simply a loss-of-function mutation. *Rhbdf2*$^{-/-}$ mice failed to recapitulate the *Rhbdf2*^{cub} phenotype. In addition, we demonstrate that similar to the *Rhbdf2*^{cub} mutation, dominant missense mutations in the N terminus of iRhom2 induce secretion of AREG and HB-EGF in a manner mediated by key amino acids in transmembrane helices 2, 4, and 6 of the peptidase domain. Thus, our results suggest that the cytosolic N terminus of iRhom2 negatively regulates EGFR signaling by suppressing the peptidase domain and, consequently, secretion of AREG/HB-EGF (Fig. 8). These findings are consistent with a recent study suggesting that in mammalian cells, whereas the cytosolic domain of Derlin-1, a novel rhomboid pseudoprotease, is essential for clearance of misfolded proteins from the endoplasmic reticulum, the transmembrane domain is required to interact with its substrates (2). Our findings also reveal more subtle regulatory functions for iRhom2 that are unmasked in N-terminal mutations, such as *Rhbdf2*^{cub}.

Instead, the *Rhbdf2*^{cub} may be considered a gain-of-function mutation. This conclusion is supported by several pieces of evidence. First, the negative regulatory role of iRhom2 seems to be minimal because *Rhbdf2*$^{-/-}$ mice do not present an overt "EGFR hyperactive" phenotype except when combined with the *Rhbdf2*^{cub} mutation. Second, cotransfection of Hu*Cub* and *AREG* results in approximately two- to threefold greater levels of AREG compared with transfections of either Hu*Wt* and *AREG* or *AREG* alone. Third, expression of Hu*Cub* induced secretion of membrane-anchored AREG and HB-EGF independent of metalloprotease activity. Fourth, mutant iRhom2 alleles fail to induce secretion of AREG/HB-EGF in the absence of the peptidase domain. Consistent with these observations, transgenic expression of the N-terminal–truncated but not full-length *RHBDF1* induces a strong EGFR signaling-related wing phenotype in *Drosophila*. Additionally, coexpression of truncated *RHBDF1* with *HB-EGF* intensifies the altered wing phenotype in *Drosophila*, indicating that the truncated iRhom1 might induce secretion of HB-EGF (32), and thereby activate EGFR signaling. These

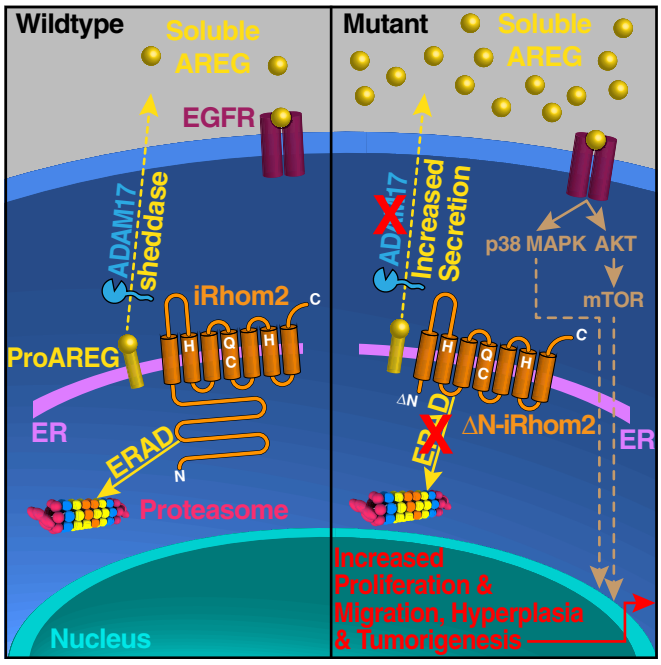

Fig. 8. Working model for our study shows that WT iRhom2 is a short-lived protein, whereas loss of its N terminus or mutations in its N-terminal domain, including those that underlie epithelial cancers, increase its protein stability. Increased protein stability, in turn, augments the secretion of selective EGF family ligands, including AREG. Inhibition of ADAM17 has no effect on AREG secretion, whereas loss of amino acids H366, Q426, C432, and H475 in the peptidase domain of iRhom2 abrogates AREG secretion. Enhanced secretion of AREG leads to hyperactivation of EGFR signaling, and thereby increased cell proliferation and migration. ER, endoplasmic reticulum; ERAD, endoplasmic reticulum associated degradation.

results validate the concept that the cytosolic N terminus contributes to iRhom-elicited ubiquitin processing of EGF family ligands, whereas the iRhom peptidase domain stimulates EGFR signaling when not suppressed by the N terminus.

It has been hypothesized that mutant iRhom2 alleles can enhance maturation of ADAM17 (6), leading to constitutive activation of EGFR signaling. However, we found that mutant iRhom2 alleles induce secretion of AREG and HB-EGF in the presence of saturating concentrations of MM, a potent broad-spectrum metalloprotease inhibitor. Maturation of other members of the ADAM family is unaffected by the deficiency of both iRhoms (9). Moreover, we demonstrate that ADAM17 activity is attenuated in *Rhbdf2*^{cub} mice. Thus, we conclude that *Rhbdf2*^{cub} and tylotic mutations selectively induce secretion of AREG and HB-EGF independent of metalloprotease activity, and that the transmembrane peptidase domain is necessary for this function.

Hyperactive EGFR Pathway Underlies Accelerated Cutaneous Healing in *Rhbdf2*^{cub} Mice. The biology of wound healing is complex. In human adults, wounds are vulnerable to nonfunctional fibrotic tissue formation, whereas wounds occurring during the prenatal period accomplish complete regeneration, resembling scar-free healing in vertebrates, such as axolotls and planarians. Even though the highly orchestrated and rapid events that occur following injury are well documented, the tissue regeneration and remodeling field is still in its infancy. The literature suggests that a strong link exists between rhomboid proteases and cutaneous wound healing. Active rhomboid RHBDL2 has been demonstrated to induce cell proliferation and migration by specifically cleaving EGF, thrombomodulin, and EphrinB3 (33, 44, 45). In vitro wound-healing assays performed in a human keratinocyte cell line indicate that the expression of *RHBDL2* is significantly up-regulated after wounding compared with unwounded controls. Also, increased *RHBLD2* expression correlates with increased shedding of membrane-bound thrombomodulin (46). Although these results suggest that targeting rhomboid proteases might have a therapeutic benefit in impaired cutaneous healing, the physiological substrates of rhomboid proteases are still unclear.

In several mouse models of wound healing, including the "superhealing" Murphy–Roths–Large (MRL/MpJ) strain, studies have shown that excessive inflammation delays healing, whereas rapid reepithelialization and reduced inflammation lead to accelerated and scar-free healing (15, 47–51). The ability of *Rhbdf2*^{cub} mice to heal wounds rapidly without significant scar formation might be due to a combination of decreased TNF-α secretion due to attenuated ADAM17 activity and rapid reepithelialization induced by augmented AREG production/EGFR hyperactivation. We propose that although decreased TNF-α contributes to a lesser degree of inflammation, increased AREG production facilitates accelerated proliferation and migration of keratinocytes to the wound site in *Rhbdf2*^{cub} mice. Moreover, iRhom2 is predominantly expressed in the skin, making it a potential therapeutic target in impaired cutaneous wound healing.

iRhom2-AREG-EGFR Pathway Is Constitutively Active in Some Epithelial Cancers. Several studies have implicated iRhom mutations in cancer. For example, overexpression of the *RHBDF1* gene, which encodes iRhom1, is crucial in sustaining growth signaling in epithelial cancer cells (4, 5). Significant elevation of *RHBDF1* transcript levels is observed in breast cancer clinical specimens. Although iRhom1 suppresses secretion of EGF family ligands and negatively regulates EGFR signaling (3), a recent study suggests that iRhom1 might have additional physiological roles (9). For instance, it has been implicated in G protein-coupled receptor transactivation of the EGFR signaling pathway (5). Moreover, unlike iRhom2 KO mice, iRhom1 KO mice have a more severe phenotype and survive for about 6 wk (9).

In humans, dominant mutations in the N terminus of the *RHBDF2* gene are associated with hyperkeratosis and esophageal cancer (11, 42). Although the mechanisms underlying the pathogenesis of hyperkeratosis and cancer are unclear, analyses of skin biopsies of patients suggest constitutive EGFR activation. Specifically, EGFR levels were shown to be significantly lower in tylotic keratinocytes compared with control keratinocytes, implicating excessive or prolonged activation-induced down-regulation of EGFR (11). Interestingly, because the *RHBDF2* mutations described to date arose in the N terminus, dominant mutations in the N terminus of iRhom2 could trigger esophageal cancer via an EGFR-dependent signaling event. In the present study, we find that N-terminal–truncated iRhom2 promotes increased AREG production independent of ADAM17 activity, and thereby induces EGFR activation. In particular, the phenotype of *Apc*$^{Min/+}$ *Rhbdf2*$^{+/cub}$ mice recapitulates the increased susceptibility to epithelial cancers seen in patients with dominant *RHBDF2* mutations (11, 42). However, *Rhbdf2*$^{cub/cub}$ mice did not spontaneously develop tumors, suggesting that the *Rhbdf2*^{cub} mutation might not drive cancer development but, instead, might promote tumor growth and progression by creating a conducive environment.

Materials and Methods

Full details are available in *SI Materials and Methods*.

Mice were obtained, bred, and maintained under modified barrier conditions at The Jackson Laboratory. All genotypes, including *cub* and *Mcub*, were maintained on the C57BL/6J (B6) genetic background. To generate *Rhbdf2*$^{-/-}$ mice, ES cell clones (EPD0208_1_A09) obtained from the KOMP repository were injected into B6-*Tyr*^{c} (B6 albino) blastocysts. Males display-

ing >50% chimerism were mated to B6 albino females; black offspring were genotyped by PCR. Heterozygotes were mated with each other to produce homozygotes, or with *Rhbdf2*$^{cub/cub}$ mice to produce *Rhbdf2*$^{-/cub}$ mice. The Animal Care and Use Committee at The Jackson Laboratory approved all of the experimental procedures.

ACKNOWLEDGMENTS. We thank scientific services at The Jackson Laboratory core facilities for assistance with microinjections, gene expression, sequencing, and histology. We thank Bruce Gott and Michelle Farley for exceptional maintenance of mouse colonies and Bonnie Lyons, Hannah Webber, Jesse Hammer, and Rosalinda Doty for technical assistance. We are indebted to David V. Serreze, Gregory A. Cox, and Anna Lisa Lucido for comments on the manuscript and to Krish Kizhatil for helpful advice. This study was supported by National Institutes of Health Grants CA034196 (Cancer Core), HLO77642 (to L.D.S.), and DK057199 (to L.D.S.). V.H. is supported by a fellowship from the Juvenile Diabetes Research Foundation International.

1. Adrain C, Freeman M (2012) New lives for old: Evolution of pseudoenzyme function illustrated by iRhoms. *Nat Rev Mol Cell Biol* 13(8):489–498.
2. Greenblatt EJ, Olzmann JA, Kopito RR (2011) Derlin-1 is a rhomboid pseudoprotease required for the dislocation of mutant α-1 antitrypsin from the endoplasmic reticulum. *Nat Struct Mol Biol* 18(10):1147–1152.
3. Zettl M, Adrain C, Strisovsky K, Lastun V, Freeman M (2011) Rhomboid family pseudoproteases use the ER quality control machinery to regulate intercellular signaling. *Cell* 145(1):79–91.
4. Yan Z, et al. (2008) Human rhomboid family-1 gene silencing causes apoptosis or autophagy to epithelial cancer cells and inhibits xenograft tumor growth. *Mol Cancer Ther* 7(6):1355–1364.
5. Zou H, et al. (2009) Human rhomboid family-1 gene RHBDF1 participates in GPCR-mediated transactivation of EGFR growth signals in head and neck squamous cancer cells. *FASEB J* 23(2):425–432.
6. Maretzky T, et al. (2013) iRhom2 controls the substrate selectivity of stimulated ADAM17-dependent ectodomain shedding. *Proc Natl Acad Sci USA* 110(28):11433–11438.
7. Adrain C, Zettl M, Christova Y, Taylor N, Freeman M (2012) Tumor necrosis factor signaling requires iRhom2 to promote trafficking and activation of TACE. *Science* 335(6065):225–228.
8. McIlwain DR, et al. (2012) iRhom2 regulation of TACE controls TNF-mediated protection against Listeria and responses to LPS. *Science* 335(6065):229–232.
9. Christova Y, Adrain C, Bambrough P, Ibrahim A, Freeman M (2013) Mammalian iRhoms have distinct physiological functions including an essential role in TACE regulation. *EMBO Rep* 14(10):884–890.
10. Etheridge SL, Brooke MA, Kelsell DP, Blaydon DC (2013) Rhomboid proteins: A role in keratinocyte proliferation and cancer. *Cell Tissue Res* 351(2):301–307.
11. Blaydon DC, et al. (2012) RHBDF2 mutations are associated with tylosis, a familial esophageal cancer syndrome. *Am J Hum Genet* 90(2):340–346.
12. Guichard A, et al. (1999) rhomboid and Star interact synergistically to promote EGFR/MAPK signaling during Drosophila wing vein development. *Development* 126(12):2663–2676.
13. Sturtevant MA, Roark M, Bier E (1993) The Drosophila rhomboid gene mediates the localized formation of wing veins and interacts genetically with components of the EGF-R signaling pathway. *Genes Dev* 7(6):961–973.
14. Hansen LA, et al. (1997) Genetically null mice reveal a central role for epidermal growth factor receptor in the differentiation of the hair follicle and normal hair development. *Am J Pathol* 150(6):1959–1975.
15. Werner S, Grose R (2003) Regulation of wound healing by growth factors and cytokines. *Physiol Rev* 83(3):835–870.
16. Normanno N, et al. (2006) Epidermal growth factor receptor (EGFR) signaling in cancer. *Gene* 366(1):2–16.
17. Johnson KR, et al. (2003) Curly bare (cub), a new mouse mutation on chromosome 11 causing skin and hair abnormalities, and a modifier gene (mcub) on chromosome 5. *Genomics* 81(1):6–14.
18. Luetteke NC, et al. (1994) The mouse waved-2 phenotype results from a point mutation in the EGF receptor tyrosine kinase. *Genes Dev* 8(4):399–413.
19. Mann GB, et al. (1993) Mice with a null mutation of the TGF alpha gene have abnormal skin architecture, wavy hair, and curly whiskers and often develop corneal inflammation. *Cell* 73(2):249–261.
20. Sorkin A, Goh LK (2009) Endocytosis and intracellular trafficking of ErbBs. *Exp Cell Res* 315(4):683–696.
21. Madshus IH, Stang E (2009) Internalization and intracellular sorting of the EGF receptor: a model for understanding the mechanisms of receptor trafficking. *J Cell Sci* 122(Pt 19):3433–3439.
22. Henriksen L, Grandal MV, Knudsen SL, van Deurs B, Grøvdal LM (2013) Internalization mechanisms of the epidermal growth factor receptor after activation with different ligands. *PLoS ONE* 8(3):e58148.
23. Fraguas S, Barberán S, Cebrià F (2011) EGFR signaling regulates cell proliferation, differentiation and morphogenesis during planarian regeneration and homeostasis. *Dev Biol* 354(1):87–101.
24. Jiang H, Grenley MO, Bravo MJ, Blumhagen RZ, Edgar BA (2011) EGFR/Ras/MAPK signaling mediates adult midgut epithelial homeostasis and regeneration in Drosophila. *Cell Stem Cell* 8(1):84–95.
25. Tokumaru S, et al. (2000) Ectodomain shedding of epidermal growth factor receptor ligands is required for keratinocyte migration in cutaneous wound healing. *J Cell Biol* 151(2):209–220.
26. Richardson GD, et al. (2009) KGF and EGF signalling block hair follicle induction and promote interfollicular epidermal fate in developing mouse skin. *Development* 136(13):2153–2164.
27. Cook PW, et al. (1991) A heparin sulfate-regulated human keratinocyte autocrine factor is similar or identical to amphiregulin. *Mol Cell Biol* 11(5):2547–2557.
28. Schneider MR, Werner S, Paus R, Wolf E (2008) Beyond wavy hairs: The epidermal growth factor receptor and its ligands in skin biology and pathology. *Am J Pathol* 173(1):14–24.
29. Stoll SW, et al. (2010) Metalloproteinase-mediated, context-dependent function of amphiregulin and HB-EGF in human keratinocytes and skin. *J Invest Dermatol* 130(1):295–304.
30. Berasain C, et al. (2005) Amphiregulin: An early trigger of liver regeneration in mice. *Gastroenterology* 128(2):424–432.
31. Shao J, Sheng H (2010) Amphiregulin promotes intestinal epithelial regeneration: Roles of intestinal subepithelial myofibroblasts. *Endocrinology* 151(8):3728–3737.
32. Nakagawa T, et al. (2005) Characterization of a human rhomboid homolog, p100hRho/RHBDF1, which interacts with TGF-alpha family ligands. *Dev Dyn* 233(4):1315–1331.
33. Adrain C, et al. (2011) Mammalian EGF receptor activation by the rhomboid protease RHBDL2. *EMBO Rep* 12(5):421–427.
34. Le Gall SM, et al. (2009) ADAMs 10 and 17 represent differentially regulated components of a general shedding machinery for membrane proteins such as transforming growth factor alpha, L-selectin, and tumor necrosis factor alpha. *Mol Biol Cell* 20(6):1785–1794.
35. Fridman JS, et al. (2007) Selective inhibition of ADAM metalloproteases as a novel approach for modulating ErbB pathways in cancer. *Clin Cancer Res* 13(6):1892–1902.
36. Fleig L, et al. (2012) Ubiquitin-dependent intramembrane rhomboid protease promotes ERAD of membrane proteins. *Mol Cell* 47(4):558–569.
37. Siggs OM, et al. (2012) iRhom2 is required for the secretion of mouse TNFα. *Blood* 119(24):5769–5771.
38. Issuree PD, et al. (2013) iRHOM2 is a critical pathogenic mediator of inflammatory arthritis. *J Clin Invest* 123(2):928–932.
39. Franzke CW, et al. (2012) Epidermal ADAM17 maintains the skin barrier by regulating EGFR ligand-dependent terminal keratinocyte differentiation. *J Exp Med* 209(6):1105–1119.
40. Peschon JJ, et al. (1998) An essential role for ectodomain shedding in mammalian development. *Science* 282(5392):1281–1284.
41. Cook PW, et al. (1997) Transgenic expression of the human amphiregulin gene induces a psoriasis-like phenotype. *J Clin Invest* 100(9):2286–2294.
42. Saarinen S, et al. (2012) Analysis of a Finnish family confirms RHBDF2 mutations as the underlying factor in tylosis with esophageal cancer. *Fam Cancer* 11(3):525–528.
43. Yekkala K, Baudino TA (2007) Inhibition of intestinal polyposis with reduced angiogenesis in ApcMin/+ mice due to decreases in c-Myc expression. *Mol Cancer Res* 5(12):1296–1303.
44. Lohi O, Urban S, Freeman M (2004) Diverse substrate recognition mechanisms for rhomboids; thrombomodulin is cleaved by Mammalian rhomboids. *Curr Biol* 14(3):236–241.
45. Pascall JC, Brown KD (2004) Intramembrane cleavage of ephrinB3 by the human rhomboid family protease, RHBDL2. *Biochem Biophys Res Commun* 317(1):244–252.
46. Cheng TL, et al. (2011) Functions of rhomboid family protease RHBDL2 and thrombomodulin in wound healing. *J Invest Dermatol* 131(12):2486–2494.
47. Eming SA, Krieg T, Davidson JM (2007) Inflammation in wound repair: Molecular and cellular mechanisms. *J Invest Dermatol* 127(3):514–525.
48. Ueno M, et al. (2005) Accelerated wound healing of alkali-burned corneas in MRL mice is associated with a reduced inflammatory signature. *Invest Ophthalmol Vis Sci* 46(11):4097–4106.
49. Zins SR, Amare MF, Anam K, Elster EA, Davis TA (2010) Wound trauma mediated inflammatory signaling attenuates a tissue regenerative response in MRL/MpJ mice. *J Inflamm (Lond)* 7:25.
50. Heber-Katz E, Gourevitch D (2009) The relationship between inflammation and regeneration in the MRL mouse: Potential relevance for putative human regenerative (scarless wound healing) capacities? *Ann N Y Acad Sci* 1172:110–114.
51. Ashcroft GS, et al. (1999) Mice lacking Smad3 show accelerated wound healing and an impaired local inflammatory response. *Nat Cell Biol* 1(5):260–266.